Unexpected thermoelectric behavior and immiscibility of the allegedly complete solid solution $Sr(Ru_{1-x}Ti_x)O_3$

Hyejin Jang,[1] Jochen Brendt,[2] Laxmi N. Patro,[1] Manfred Martin,[1,2] and Han-Ill Yoo[1]

[1]*Department of Materials Science and Engineering, Seoul National University, Seoul 151-744, Republic of Korea*

[2]*Institute of Physical Chemistry, RWTH Aachen University and JARA-FIT, Aachen, Germany*

(Received 8 January 2014; revised manuscript received 18 March 2014; published 15 April 2014)

$SrRuO_3$, a p-type metallic conductor with a small thermopower, and $SrTiO_3$, a p-type insulator with a large thermopower in its hyperstoichiometric state, have been reported to make a complete solid solution. It is, thus, suggested that the thermoelectric power factor, conductivity times thermopower squared ($\sigma\theta^2$), may be best optimized by mixing these two extreme oxides. In order to explore this possibility, we examined σ and θ of the solution $Sr(Ru_{1-x}Ti_x)O_3$ against composition ($0 \leqslant x \leqslant 1$), temperature ($300 \leqslant T/K < 1000$) and oxygen activity ($-4 \leqslant \log a_{O_2} < 0$), and subsequently its crystallographic structure against x at room temperature. It has been found that, contrary to literature, there falls a miscibility gap over the composition range $0.1 < x < 0.6$. While there occurs a metal-to-insulator transition crossing the miscibility gap, θ remains little dependent on T and a_{O_2} for the compositions up to $x = 0.9$. Unexpectedly, however, θ changes its sign twice with increasing x, indicating the majority carrier type changes from p to n at a composition in $0.6 < x < 0.9$ and back to p at a composition in $0.9 < x < 1.0$, whereas σ decreases monotonically. The highest power factor is observed, contrary to the expectation, at $x = 0$ (pure $SrRuO_3$) on the order of 10^{-4} W/mK^2. The origin of the repeated carrier-type changes is discussed in terms of electronic-structure change.

DOI: 10.1103/PhysRevB.89.144107 PACS number(s): 72.20.Pa, 61.05.cj

I. INTRODUCTION

Thermoelectric power generation, that directly converts waste heat into electrical work, has been newly attracting worldwide attention for its environmentally friendly nature even though its conversion efficiency is still not high enough. The conversion efficiency is mostly determined by the thermoelectric figure-of-merit ZT of thermoelectric materials, where T is the operation temperature and $Z = \sigma\theta^2/\kappa$ with σ, θ, and κ being, respectively, the electrical conductivity, thermopower, and thermal conductivity. A higher efficiency requires a higher ZT value, but these three transport properties are mutually contradicting, thus, hindering the materials from exhibiting their ZT values far beyond unity [1].

Up to now, intermetallic compounds, e.g., Bi-Te alloys, exhibit the best thermoelectric performance, but simultaneously possess several drawbacks such as toxicity, high production cost, and poor oxidation resistance [1]. As regards oxides, on the other hand, their potential as thermoelectric materials seems to have been underestimated mainly because of their relatively poor transport properties [2]. They, nevertheless, still have some unbeatable inherent advantages that can not be easily given up: excellent oxidation resistance and high-temperature stability, among others, enabling high-temperature applications above 700 K. It is, thus, essential to enhance Z by ingeniously adjusting these conflicting transport properties of the thermoelectric oxides for their high-temperature applications.

Although those transport properties are interdependent, a strategy of developing the oxide thermoelectrics may be twofold, namely, on one hand to enhance the power factor ($\theta^2\sigma$) via defect-chemical engineering and on the other hand to suppress the thermal conductivity (κ) via microstructural engineering. This study is concerned with the former. A most common or routine methodology is to dope prospective oxides with aliovalent impurities so as to adjust charge-carrier concentration as exemplified by the cases of Nb-doped $CaMnO_3$ [3] and La-doped $SrTiO_3$ [4]. Effectiveness of this method, however, seems to be limited mainly by the solubility limit of the dopants [5]. Therefore, a new approach is necessitated, and here we explore the possibility of homogeneous solutions between two extreme oxides, one with superior conductivity but naturally inferior thermopower, and the other with superior thermopower but naturally inferior conductivity. It is expected that the power factor may then be best optimized at an intermediate composition.

We have chosen the solid solution $Sr(Ru_{1-x}Ti_x)O_3$ for $SrRuO_3$ is a most conductive p-type metallic conductor with a small thermopower on the order of 10 μV/K and hyperstoichiometric $SrTiO_3$ a wide-band-gap p-type semiconductor with a large thermopower on the order of 1 mV/K. These two end-member oxides are reported to form complete solid solution from end to end [6,7], and these solutions have been investigated intensively in view of metal-insulator transition at low temperatures [8]. The thermoelectric properties of these solutions, however, have never been examined, whereas those of the end members have been investigated rather extensively [2,9,10]. We expected a novel hybrid of the superior conductivity of ruthenite and the superior thermopower of titanate.

We, thus, examined the electrical conductivity and thermoelectric power of $Sr(Ru_{1-x}Ti_x)O_3$ solid solution against composition ($x = 0.0, 0.3, 0.6, 0.9$, and 1.0), temperature from room temperature up to ca. 1000 K and oxygen partial pressure from 1 atm down to ca. 10^{-4} atm. In this course of work, we have observed an absolutely unexpected thermoelectric behavior: while the conductivity varies just monotonically with increasing x as was originally expected, the solution of $x = 0.9$ abruptly turns to n type while all other investigated compositions remain p type. We suspected that it might be attributed to the possible change of crystallographic structure and/or valence changes of the cations and, hence, examined their structures using x-ray diffraction (XRD) and extended

x-ray absorption fine structure spectroscopy (EXAFS), and their cationic valence states by investigating the x-ray absorption near edge structure (XANES). In this course of work, we have found, contrary to the literature [6,7], that the system does not make a complete solid solution at all. We hereby report on these unexpected results in detail and discuss the origin of the carrier-type changes of p type to n type and back to p type with increasing x. Finally, we will discuss whether the solid-solution idea for power-factor tailoring is feasible.

II. EXPERIMENT

Polycrystalline $Sr(Ru_{1-x}Ti_x)O_3$ specimens of $x = 0.0, 0.3, 0.6, 0.9$, and 1.0 were prepared via a conventional solid-state reaction route: the mixtures of $SrCO_3$, RuO_2 (preheated at 873 K) and TiO_2 in appropriate ratios were calcined at 1073–1273 K in air. After intermediate grindings, the calcined powders were pressed into bars, followed by cold-isostatic pressing under 200 MPa. Sintering was subsequently carried out in air at 1573, 1623, 1673, 1793, and 1793 K for $x = 0.0$, 0.3, 0.6, 0.9, and 1.0, respectively, and cooled to ambient temperature at a rate of 2 K/min to avoid thermal shock. Sintering durations were 50 h for $x = 0.0$, 0.3, and 0.6, and 12 h for $x = 0.9$ and 1.0, resulting in sintering densities of 67%, 67%, 91%, 96%, and 96% for $x = 0.0$, 0.3, 0.6, 0.9, and 1.0, respectively, as estimated by the Archimedes method. For the purpose of phase analyses, additional samples of $x = 0.1$, 0.2, and 0.5, respectively, were later synthesized in the same way as the specimen $x = 0.3$.

The crystal-structure analyses were performed on the as-sintered specimens by powder x-ray diffraction with monochromatic Cu $K\alpha 1$ radiation (Bruker diffractometer, D8-Advance) at room temperature. High-resolution synchrotron XRD measurements were also performed on two compositions $x = 0.3$ and 0.6 in the range of 15°–135° at a step size of 0.005° by using the BL-8C2 beam line (1.5455 Å) of the Pohang Accelerator Laboratory, Korea. The Rietveld analyses were subsequently made using the GSAS program [11].

X-ray absorption spectra at the Ti, Ru, and Sr K edges were measured using the beamline C1 at the synchrotron DORIS (HASYLAB, Hamburg) in transmission geometry. The beamline is equipped with a Si (111) double-crystal monochromator and ionization chambers as detectors. In order to filter higher harmonics, the monochromator was detuned to 70% of the maximum intensity. Samples were prepared by mixing the powders of the as-sintered $Sr(Ru_{1-x}Ti_x)O_3$ with boron nitride (BN) and pressing the mixture to pellets. As the energy reference, pellets of TiO_2, RuO_2, and SrO diluted with BN were used. The spectra were measured from 300 eV below each edge to 1000 eV above the edges, measuring with high accuracy (4 data points/eV) around the edges for getting high-resolution XANES information. In the EXAFS region, a resolution of 1 data point/eV was used. Raw data analysis and fitting routines were done with IFEFFIT program package [12] according to the standard procedures [13].

Electrical conductivity and thermopower were simultaneously measured, against temperature in the range of $300 \leqslant T/K \leqslant 973$ in air and against oxygen activity in the range of $10^{-4} \leqslant a_{O_2} < 1$ at 973 K, on the parallelepiped specimens cut out of the as-sintered pallets by the four-probe dc method and steady-state technique, respectively. For experimental details, the reader is referred to Ref. [14]. The oxygen activity in the surrounding was controlled by using gas mixtures of Ar and O_2, and monitored with an *in situ* zirconia-based oxygen sensor.

III. RESULTS AND DISCUSSIONS

A. Crystal structure investigated by XRD

Figure 1(a) shows the XRD patterns of $Sr(Ru_{1-x}Ti_x)O_3$ specimens with $x = 0.0$, 0.1, 0.2, 0.3, and 0.5, respectively. They all exhibit splitting of Bragg reflections indicative of the orthorhombic characteristics of these compositions. The XRD pattern for $x = 0.1$ is essentially identical to that of orthorhombic $SrRuO_3$ with a space group *Pnma* as compiled by JCPDS, indicating that the solution of $x = 0.1$ is a single phase with orthorhombic structure. It is, however, noted that as the Ti content x increases from $x = 0.2$ to 0.5, there emerges an extra peak at $2\theta \approx 40°$ which is a characteristic peak for (111) of cubic $SrTiO_3$ with a space group $Pm\bar{3}m$. This indicates that the solutions $x = 0.2$, 0.3, and 0.5 are not of single phase, but two-phase mixtures of *Pnma* and $Pm\bar{3}m$.

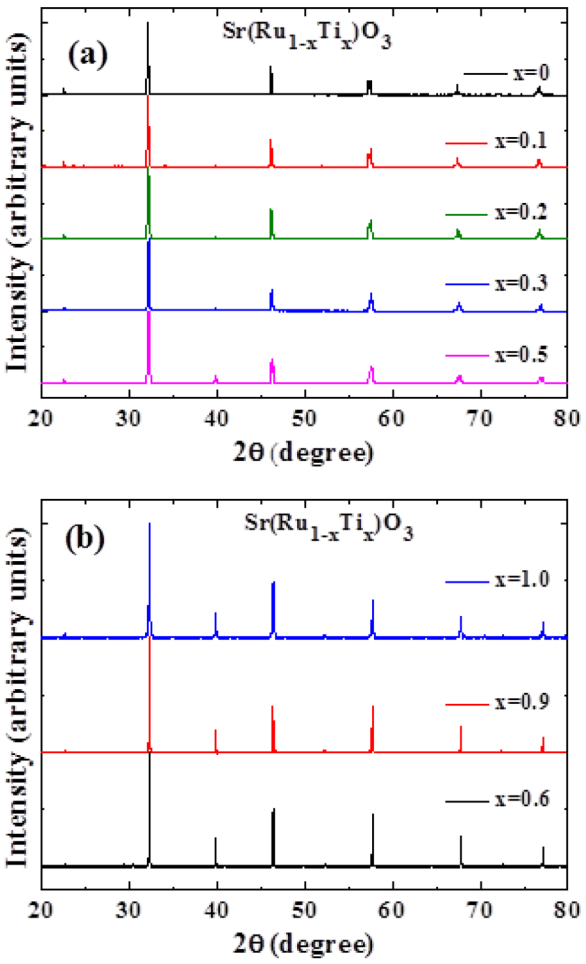

FIG. 1. (Color online) XRD patterns of $Sr(Ru_{1-x}Ti_x)O_3$ as measured at room temperature (a) for the compositions $x = 0.1$, 0.2, 0.3, 0.5; (b) for the compositions $x = 0.6$, 0.9, 1.0.

XRD patterns of the solutions $x = 0.6$, 0.9, and 1.0 are shown in Fig. 1(b). One can see that the diffraction peaks are all sharp with no splitting at all. Furthermore, the patterns for $x = 0.6$ and 0.9 are essentially the same as that of cubic $SrTiO_3$ as compiled by JCPDS No. 35-0734. This indicates that the solutions $x = 0.6$, 0.9, and 1.0 are all of single-phase cubic ($Pm\bar{3}m$). It is, thus, unavoidable to conclude that the system does by no means make a complete solution and there falls a miscibility gap over the composition range $0.10 < x < 0.60$, with 100% confidence, at room temperature at least.

Rietveld refinement results on all compositions (not shown) reconfirm the space group for $x = 0$ ($SrRuO_3$) to be *Pnma* and that for $x = 0.6$, 0.9, and 1.0 to be $Pm\bar{3}m$ in agreement with the literature [6,7].

Figure 2 shows the results of the high-resolution synchrotron XRD measurement followed by Rietveldt refinement for (a) $x = 0.6$ and (b) $x = 0.3$. The statistical goodness of fitting (χ^2) for $x = 0.6$ and 0.3 are 6.2% and 7.5%, respectively. The results confirm once again that the solution $x = 0.6$ comprises the single-phase cubic ($Pm\bar{3}m$) with lattice parameters $a = b = c = 3.8989(1)$ Å; the solution $x = 0.3$, the two phases of orthorhombic (*Pnma*) and cubic ($Pm\bar{3}m$) with phase fractions of 0.73 and 0.27, respectively. The latter in association with the lower and upper bounds of the miscibility gap $0.1 < x < 0.6$ as found from Fig. 1 allows one to best estimate the gap to be $0.19 \leqslant x \leqslant 0.59$.

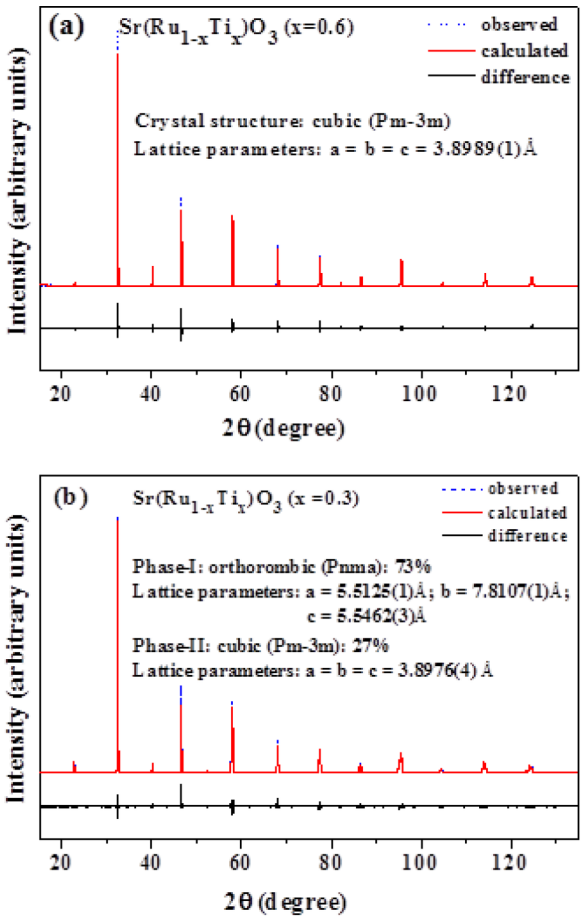

FIG. 2. (Color online) The observed and calculated XRD patterns of $Sr(Ru_{1-x}Ti_x)O_3$ for (a) $x = 0.6$ and (b) $x = 0.3$.

Actually, it has been intuitively expected that the system $(1\text{-}x)SrRuO_3 + xSrTiO_3$ may not make a complete solution because the end members already have different crystal structures, orthorhombic (*Pnma*) and cubic ($Pm\bar{3}m$) at room temperature. The earlier studies [6,7], however, have reported that this system makes a complete solution although there remains some ambiguity with respect to the structural transition with composition: Cuffini *et al.* [6] have reported that the transition from orthorhombic to cubic occurs at $0.5 < x < 0.6$, whereas Bianchi *et al.* [7] have reported that there falls an intermediate single-phase region of tetragonal ($I4/mm$) in $0.6 < x < 0.7$ upon transition from *Pnma* to $Pm\bar{3}m$. This type of orthorhombic-to-tetragonal transition is frequently observed in octahedral-tilting perovskite oxides and the transition sequences are reported in detail for some materials [15–17].

As regards the end member $SrRuO_3$, Kennedy *et al.* [16] have reported from their high-resolution synchrotron diffraction studies that the orthorhombic *Pnma* at room temperature undergoes a continuous transition to *Imma* at 685 K and then a discontinuous transition to $I4/mcm$ in the vicinity of 825 K, and finally remains $Pm\bar{3}m$ above 950 K. The present system may thus be expected to likely make a complete solution only above this temperature.

The phase separation requires cation diffusion, which is well known to be extremely sluggish in these types of materials [18,19]. In this study, the time elapse (ca. 12 h) for cooling from the sintering temperature of 1623 K was very short for the sluggish diffusion and the grain sizes of the two observed phases must not be nanosized as their x-ray peak widths are very small (actually, >1 μm). Thus, phase separation as observed in this work must have taken place at much elevated temperatures.

B. Crystal structure investigated by EXAFS

More detailed insight into the crystal structures was obtained using the EXAFS technique. X-ray absorption spectra of good quality were taken near the Sr and Ru *K* edges rendering possible a structural analysis from the viewpoint of Sr, occupying A sites within the perovskite structure, and from the viewpoint of Ru, occupying B sites. In contrast, the quality of the Ti *K*-edge spectra was not sufficient for EXAFS analysis due to the strong absorption by the heavy elements Sr and Ru. Figure 3 shows the modified radial distribution functions around Ru and Sr as obtained from the EXAFS spectra.

The distribution function around Ru in Fig. 3(a) shows, in the first coordination shell that is formed by oxygen, only slight changes with changing composition x. This result confirms that the BO_6 octahedra are preserved throughout the series $Sr(Ru_{1-x}Ti_x)O_3$ ($x = 0.0$, 0.3, 0.6, 0.9) and only the B-O distance slightly increases with decreasing x. In contrast, the second and third shells around Ru (formed by Sr and Ti/Ru) show strong changes with decreasing x. This effect has two possible causes: (i) With decreasing x, i.e., increasing Ru content, the tilting of the BO_6 octahedra increases and thereby the "perfect" interferences in the cubic perovskite $SrTiO_3$

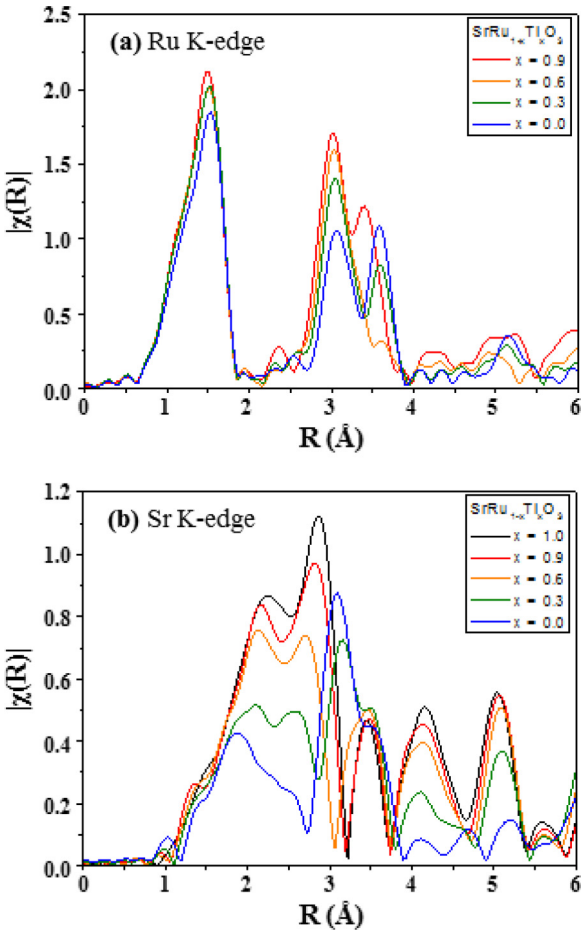

FIG. 3. (Color online) (a) Radial EXAFS distribution function around Ru for $Sr(Ru_{1-x}Ti_x)O_3$ ($x = 0.0, 0.3, 0.6$, and 0.9) as obtained from the Ru K-edge x-ray absorption spectrum. (b) Radial EXAFS distribution function around Sr for $Sr(Ru_{1-x}Ti_x)O_3$ ($x = 0.0$, 0.3, 0.6, 0.9, and 1.0) as obtained from the Sr K-edge x-ray absorption spectrum.

are destroyed, resulting in a decrease of the amplitude of the third-shell contribution to the radial distribution function (RDF). (ii) With the change of the occupation of the third shell from Ti rich to Ru rich, the backscattering amplitudes change. The changes in the RDF are much more pronounced in the distribution function around Sr [Fig. 3(b)]. The whole RDF around Sr, including the first peak, exhibits strong changes with changing composition x, as Sr occupies the A site within the perovskite structure and tilting of the BO_6 octahedra changes all angles and distances between Sr and the backscatterer atoms O and Ti/Ru, thereby destroying the "perfect" interferences in $SrTiO_3$ and decreasing all amplitudes in the RDF.

As the radial distribution function (RDF) around Sr is very sensitive to the tilting of the BO_6 octahedra, it can be used to refine the structure of orthorhombic $SrRuO_3$. Figure 4 shows the experimental RDF and several calculated RDFs where the crystallographic angles α, β, and γ are varied. Figure 4(b) corresponds the angles $\alpha = 7.4°$, $\beta = 7.1°$, and $\gamma = 5.1°$ which were taken from literature [20]. The corresponding calculated RDF shows, however, two well-separated peaks at distances of 1.8 and 2.4 Å, in contrast to the experimental RDF that exhibits only one peak. Better agreement with the experimental RDF can be obtained by changing the angles [see Figs. 4(b)–4(d)], and the optimum agreement is obtained for $\alpha = 7°$, $\beta = 6°$, and $\gamma = 2°$ [see Figs. 4(d) and 4(e)].

The XRD analysis had shown that the sample with $x = 0.3$ is not a single-phase but a two-phase mixture. This result is confirmed by the EXAFS data. Taking the spectra of the single-phase samples $SrRuO_3$ ($x = 0$) and $Sr(Ru_{0.4}Ti_{0.6})O_3$ ($x = 0.6$) as references, the EXAFS function χ(k) of the two-phase sample $Sr(Ru_{0.7}Ti_{0.3})O_3$ ($x = 0.3$) can be fitted by a linear-combination fit: $\chi_{x=0.3}(k) = a \cdot \chi_{x=0.0}(k) + (1-a) \cdot \chi_{x=0.6}(k)$. For both the Sr and Ru spectra, good-fit results are obtained [see Figs. 5(a) and 5(b)], and the phase fractions obtained from both fits a(Sr) = 0.49 and a(Ru) = 0.52 agree well. This result means that the EXAFS spectrum of the two-phase sample $Sr(Ru_{0.7}Ti_{0.3})O_3$ ($x = 0.3$) can be described sufficiently well by a 1:1 mixture of $SrRuO_3$ ($x = 0$) and $Sr(Ru_{0.4}Ti_{0.6})O_3$ ($x = 0.6$), which would correspond to a miscibility gap $0.1 < x < 0.6$ in agreement with the XRD results above. This interval is, however, only an upper bound as only a limited number of compositions could be analyzed by EXAFS, and the real miscibility gap might be smaller.

C. Transport properties

1. Against oxygen activity

Figure 6 shows the conductivities (σ) and corresponding thermopowers (θ) versus oxygen activity (a_{O_2}) for different compositions (x) of certainly single phase $Sr(Ru_{1-x}Ti_x)O_3$ ($x = 0.0$, 0.6, 0.9, 1.0) in equilibrium state at a fixed temperature of 973 K.

It is first noted that the conductivity of the composition $x = 1.0$ or $SrTiO_3$ increases with increasing oxygen activity as

$$\log(\sigma/\mathrm{Scm}^{-1}) = -(2.890 \pm 0.013) + (0.237 \pm 0.005)\log a_{O_2} \quad (1)$$

indicating a p-type conduction in accord with the sign (+) of its thermopower. This behavior is in agreement with what is expected from the defect structure of nominally pure $SrTiO_3$. In normal oxidizing atmospheres as now, it is known [21] to be governed by background acceptor impurities A'_C (typically Al'_{Ti}) and charge-compensating oxygen vacancies $V_O^{\bullet\bullet}$ or

$$[A'_C] \approx 2[V_O^{\bullet\bullet}] \quad (2)$$

in the Kröger-Vink notation [22]. The oxidation reaction equilibrium

$$\tfrac{1}{2}O_{2(g)} + V_O^{\bullet\bullet} \rightleftarrows O_O^{\times} + 2h^{\bullet} \quad (3)$$

stipulates the associated reaction equilibrium constant K_{Ox} to be

$$K_{\mathrm{Ox}} = \frac{p^2}{[V_O^{\bullet\bullet}]a_{O_2}^{1/2}} \quad (4)$$

in the ideal dilute solution regime of defect concentrations, where $p = [h^{\bullet}]$ is the concentration of holes. Equations (2)

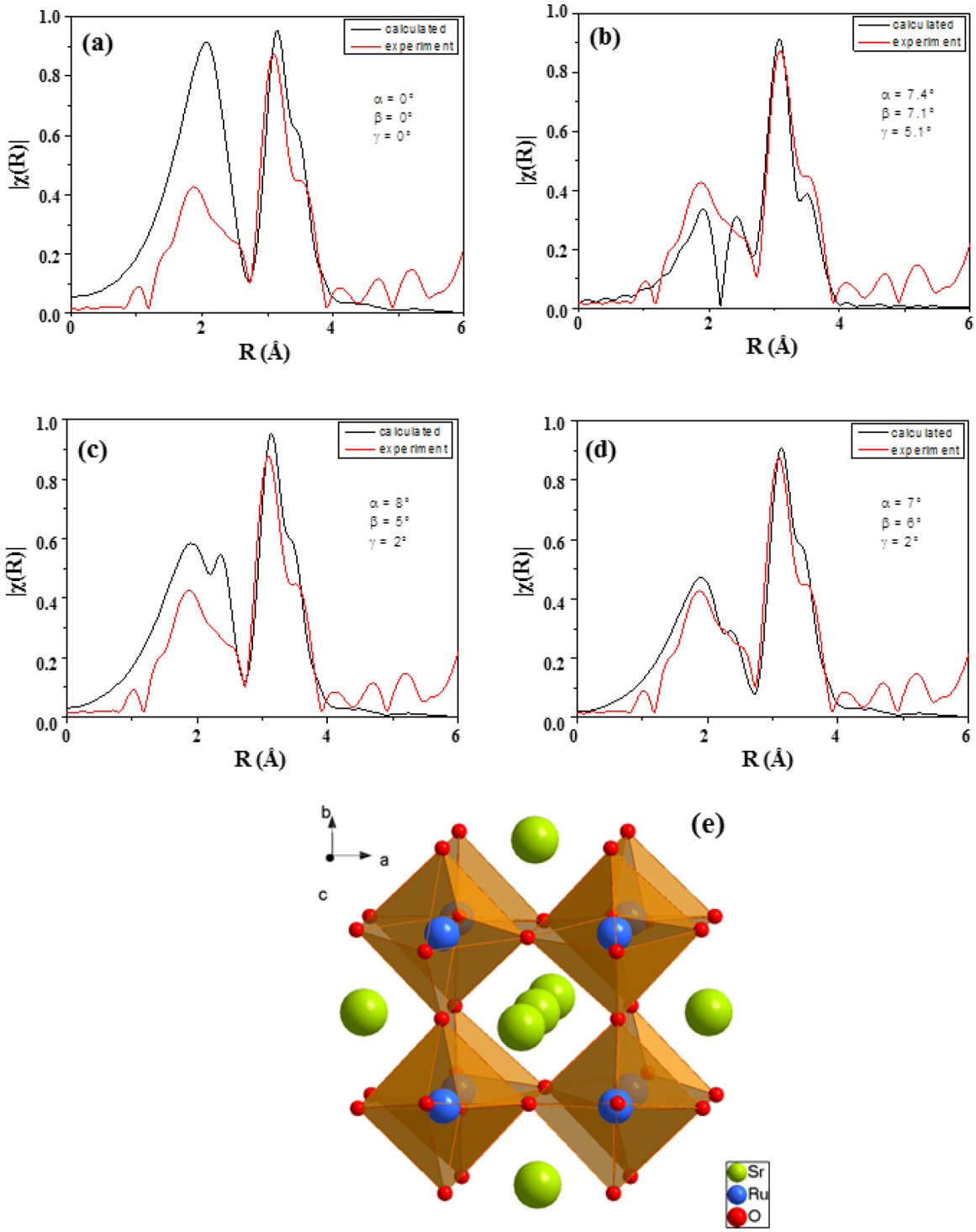

FIG. 4. (Color online) (a)–(d) Comparison of the radial distribution function (RDF) around Sr in $SrRuO_3$ as obtained experimentally (red) with the RDF as calculated for different tilting angles α, β, and γ of the BO_6 octahedra. (e) Crystal structure of $SrRuO_3$ with tilting angles $\alpha = 7°$, $\beta = 6°$, and $\gamma = 2°$ according to Fig. 4(d) (best agreement between experimental and calculated RDF around Sr).

and (4) then lead to

$$\sigma \propto p = K_{\mathrm{Ox}}^{1/2}[A'_C]^{1/2}a_{O_2}^{1/4}. \tag{5}$$

Upon comparison with Eq. (1), one can indeed see that the as-observed oxygen exponent (0.24) is quite close to the ideal value 1/4.

It is also known [21,23] that for the band conduction of exclusively p type (and exclusively n type as well), θ can be represented as

$$\theta = \frac{k}{e_o}\left(\ln\frac{N_V}{p} + A_p\right), \tag{6}$$

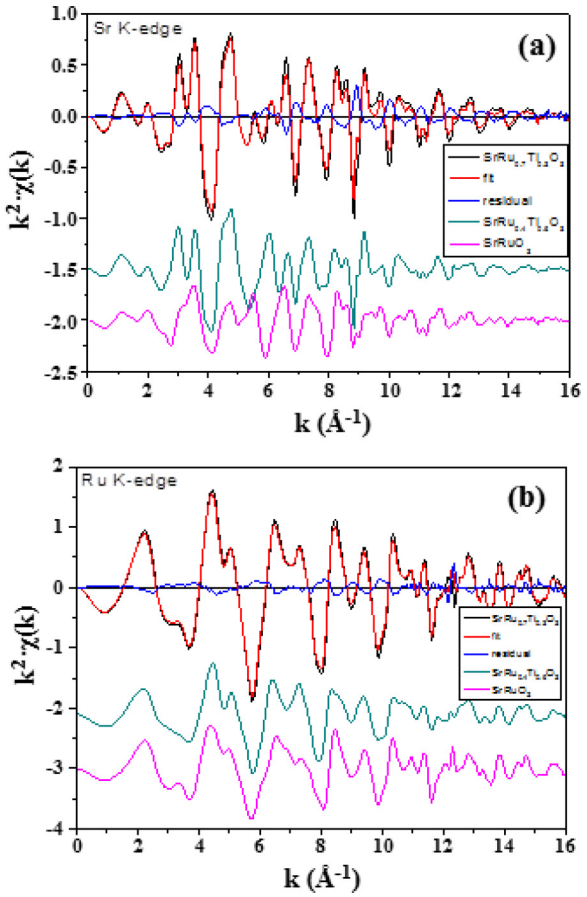

FIG. 5. (Color online) Linear combination fit of the EXAFS function $\chi_{0.3}$(k) of the two-phase sample $Sr(Ru_{0.7}Ti_{0.3})O_3$ with the EXAFS functions $\chi_{0.0}$(k) and $\chi_{0.6}$(k) of $SrRuO_3$ and $Sr(Ru_{0.4}Ti_{0.6})O_3$, respectively. (a) Sr K edge, (b) Ru K edge.

where e_o denotes the fundamental charge, k the Boltzmann constant, N_V the effective density of states at the valence band edge, and A_p a constant involving the carrier mobility and entropy of transport. As is depicted by the solid line in Fig. 6(b), the (reduced) thermopower may be best estimated as

$$\frac{e_o\theta}{2.303k} = (4.60 \pm 0.13) - (0.24 \pm 0.05)\log a_{O_2} \qquad (7)$$

with the oxygen exponent, 0.24, that is again close to the ideal value 1/4 due to Eq. (5).

Contrary to the nominally pure $SrTiO_3$, the other three (single-phase) compositions $x = 0$, 0.6, and 0.9 exhibit both properties being essentially independent of oxygen activity so that one may regard them as constant as summarized in Table I. This fact indicates that the carrier densities for these compositions are not redox generated, but of other origins anchoring the carrier density for each, e.g., internal thermal disorder or external aliovalent impurities (see later)

It is now emphasized that the thermopower signs tell that only the composition $x = 0.9$ is of n type ($\theta < 0$), whereas all the rest are of p type ($\theta > 0$). Both the end members are of p type, and hence, we expected that any solution between them would remain the same type like the composition $x = 0.6$. In this light, the unexpected carrier-type-reversal at $x = 0.9$ is quite surprising and even peculiar.

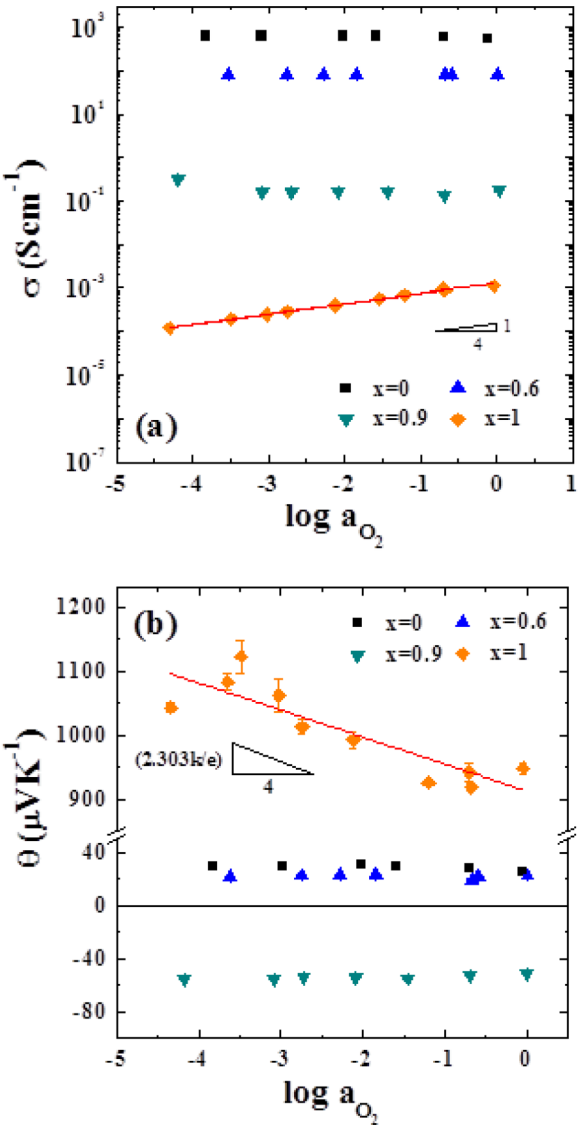

FIG. 6. (Color online) (a) Electrical conductivities and (b) thermopowers vs oxygen activity of solid solutions $Sr(Ru_{1-x}Ti_x)O_3$ with $x = 0.0$, 0.6. 0.9, and 1.0 in equilibrium state at 973 K. Solid lines for $x = 1$ are the best fitted and the small triangles show the ideal slopes: 1/4 (a) and (2.303 k/e)/4 (b) (see the text).

2. *Against temperature*

Figure 7 shows the variations of conductivity (a) and thermopower (b) against temperature for the compositions $x = 0.0$, 0.3, 0.6, 0.9, and 1.0 in a fixed oxygen activity atmosphere, air. Here, one can again see that whereas the rest

TABLE I. Oxygen-activity-independent conductivities and thermopowers of single phase $Sr(Ru_{1-x}Ti_x)O_3$ with $x = 0.0$, 0.6, and 0.9 at 973 K.

x	σ/Scm^{-1}	θ/μ VK^{-1}
0.0	597 ± 30	28.3 ± 1.7
0.6	79.7 ± 1.3	21.9 ± 1.2
0.9	0.163 ± 0.015	-54.2 ± 1.5

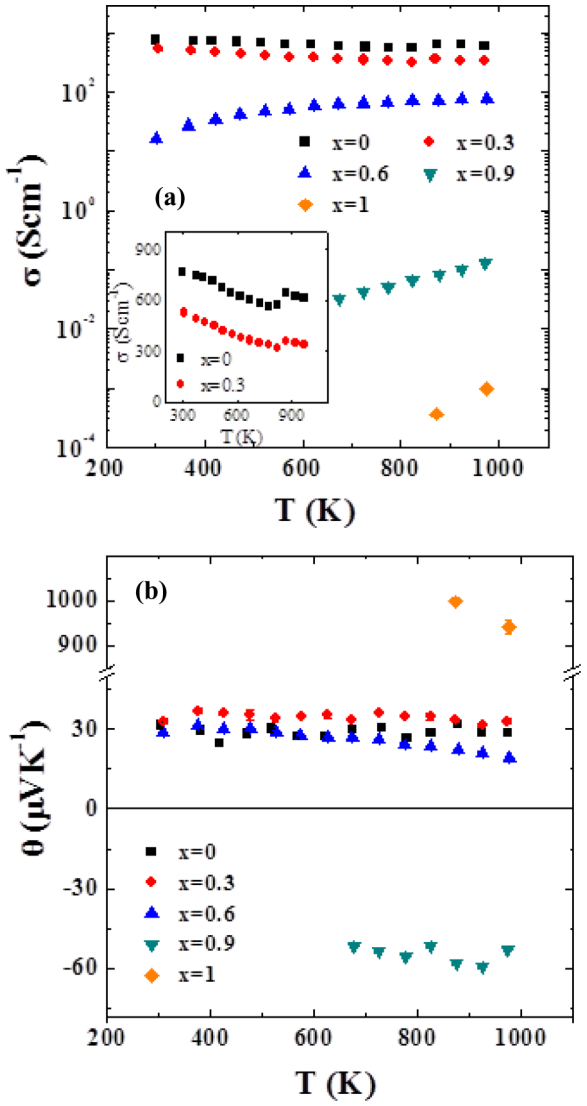

FIG. 7. (Color online) (a) Conductivity and (b) thermopower vs temperature of compositions $x = 0.0, 0.3, 0.6, 0.9$, and 1.0. The inset in (a) shows conductivity jumps at ca. 873 K for $x = 0.0$ and 0.3 in the linear conductivity scale.

remain p type ($\theta > 0$), $x = 0.9$ remains n type ($\theta < 0$) all the way.

As temperature is lowered, the present oxide systems tend to be oxidized via Eq. (2) (for the oxidation reaction is normally exothermic) providing their boundaries remain open with respect to oxygen exchange. It has, however, already been shown in Fig. 6 that the carrier densities of all the compositions except for $x = 1.0$ are not redox generated. It is therefore expected that, if not of the thermal disorder origin, the carrier densities should be independent of temperature, too. As is seen from Fig. 7(b), the thermopowers, a measure of carrier density [see, e.g., Eq. (6)], of all the compositions except for $x = 1.0$ are indeed little dependent, if not absolutely independent, on temperature, thus regarded as constant as listed in Table II. One can see that these temperature-independent values are indeed in agreement with those oxygen-activity-independent ones in Table I within experimental errors for each of the common

TABLE II. Temperature-independent thermopowers of nominal compositions $x = 0.0, 0.3, 0.6$, and 0.9.

x	θ/μ VK^{-1}
0.0	28.1 ± 2.5
0.3	34.4 ± 1.5
0.6	26.2 ± 3.6
0.9	-54.8 ± 3.1

compositions. It is thus indicated that the carriers for these compositions are not of thermal disorder origin.

Any temperature dependence of the conductivities of these compositions may then be attributed to the carrier mobility and, hence, the conduction mechanisms. The conductivities of $x = 0.0$ and 0.3 exhibit a metallic behavior or $d\sigma/dT < 0$; those of $x = 0.6$ and 0.9 a thermally activated behavior or $d\sigma/dT > 0$ with activation energies of 0.102 ± 0.005 eV and 0.26 ± 0.02 eV, respectively. These trends with temperature depending on the composition x are in general agreement with that reported [8].

Noting the composition $x = 0.3$ being a two-phase mixture consisting of roughly 60 mol% orthorhombic $Sr(Ru_{0.9}Ti_{0.1})O_3$ and the balance of cubic $Sr(Ru_{0.4}Ti_{0.6})O_3$, it is not surprising that its electrical conductivity should be not much different from that of pure ruthenite, $x = 0$.

An interesting thing is that there occurs a jump of the metallic conductivity of $x = 0.0$ and 0.3 at around 873 K [see the inset in Fig. 7(a)]. This temperature coincides with that of phase transition of pure $SrRuO_3$ from orthorhombic to tetragonal [16]. It is known [17] that the higher the crystal symmetry, the higher the degree of overlapping between the d orbital of B ions and $2p$ orbital of O ions in an ABO_3 perovskite system, enhancing its p-type conductivity. The jump for $x = 0.3$ may, thus, be attributed to the similar phase transition of the majority Ru-rich phase ($x \approx 0.1$).

3. *Against composition*

The data in Fig. 7 are replotted against composition x at selected temperatures in Fig. 8. One can see more clearly that the conductivity monotonically decreases from metallic conductivity of the order of 10^3 S/cm to an insulator level of the order of 10^{-5} S/cm, at an increasing rate as Ti fraction x increases from 0 to 1, but the thermopower varies in the unexpected way: It remains nearly flat around 30 μV/K up to $x = 0.6$, then shifts to -55 μV/K at $x = 0.9$ and finally back to ca. $+1$ mV/K at $x = 1.0$, reflecting the carrier-type changes from p type to n type at $x \approx 0.70$ and then back to p type at $x \approx 0.95$.

The changes, with increasing x, of carrier types from p to n to p as well as of conduction mechanisms from band to thermally activated back to band may be understood in terms of the gradual change of electronic structures. An end member $SrRuO_3$ ($x = 0$) is a p-type metallic conductor with the two-third-filled band of Ru t_{2g} states (low spin Ru^{4+}) that are strongly hybridized with the O-$2p$ states [24]. The other end member $SrTiO_3$ is a wide-band-gap insulator with the valence band of O-$2p$ orbitals and the conduction band consisting of empty Ti-$3d$ orbitals. The gap between these

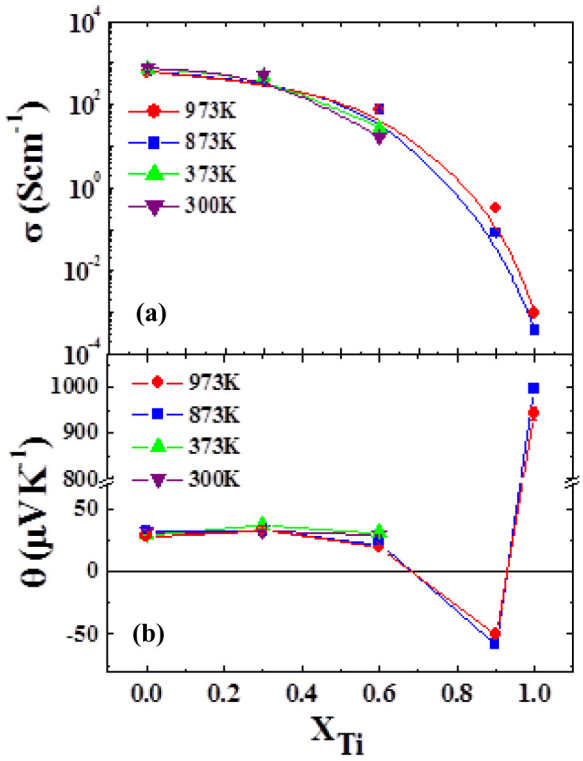

FIG. 8. (Color online) (a) Conductivity and (b) thermopower vs composition x of the system $Sr(Ru_{1-x}Ti_x)O_3$ at different temperatures in the air atmosphere. Solid lines are for visual guidance only.

bands is about 3.3 eV [25]. As these two end members form solid solutions, Ru and Ti ions are randomly mixed, but the t_{2g} states of Ru and Ti ions are well decoupled [8] with the Ru t_{2g} band at the lower energy level than the Ti t_{2g} band, thus, dominating the electronic structure near the Fermi level [8]. Therefore, the transport properties of Ru-rich samples should remain similar to that of pure $SrRuO_3$ as exemplified by the two-phase sample of $x = 0.3$. As the Ti content increases further, Ru t_{2g} orbitals are getting less and less overlapped, thus tending to form a narrow band, and hole mobility is getting energetically more and more expensive. This is believed to be the case for $x = 0.6$ which has only a few factor smaller carrier density, thus still has similar thermopower, but exhibits a hopping conduction with an activation energy of 0.1 eV in agreement with literature [8]. As the Ti content increases even further to, say, $x = 0.9$, Ru can no longer form a band, but only forms discrete impurity states (probably high-spin Ru^{4+}) just below the Ti $3d$ conduction band. Then, Ru^{4+} ions act as donors ($Ru_{Ti}^{\bullet}$), as supported by first-principles density functional theory (DFT) calculation [26], and charge is transferred via electron hopping from Ti^{3+} to Ti^{4+}, resulting in n-type conductivity. This is why the composition $x = 0.9$ has been rendered to an n type. Matsumoto *et al.* [27] have also reported on the n-type thermoelectric powers in Ru-doped $SrTiO_3$ with compositions of $x = 0.95$, 0.90, and 0.80.

If it is the case, the electronic concentration is fixed by the Ru-donor content or

$$n \approx [Ru_{Ti}^{\bullet}], \tag{8}$$

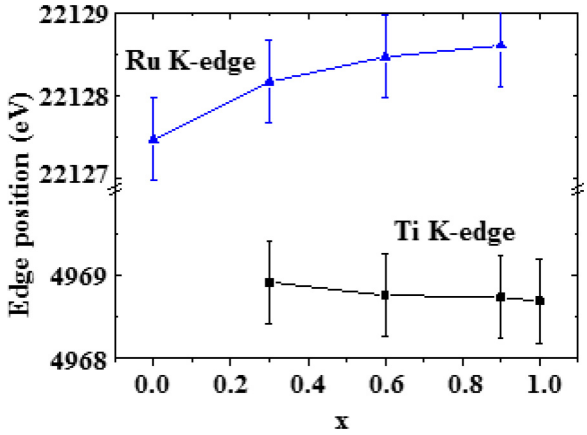

FIG. 9. (Color online) Positions of the Ti K edge and at the Ru K edge, respectively, as obtained from the XANES part of the x-ray absorption spectra for different Ti contents x in $Sr(Ru_{1-x}Ti_x)O_3$.

rendering the thermopower to be essentially constant irrespective of oxygen activity and temperature as well in their ranges examined and the conductivity to be thermally activated with an activation energy of ca. 0.2 eV, as we observed. The quantitative interpretation of the thermopower for the composition $x = 0.9$, however, is not straightforward at the moment, due to the lack of information on the transported entropy of hopping electrons or small polarons [28] in the matrix of $SrTiO_3$.

The analogous situation has been already reported on the system $Sr(Fe_{1-x}Ti_x)O_3$ [29], where Fe^{4+} ions have an electron configuration of [Ar] $3d^4$, similar to Ru^{4+} ([Kr] $4d^4$). Fe $3d$ states form a conduction band for the composition up to $x = 0.5$, whereas acceptorlike impurity states for $x = 0.99$.

XANES analysis qualitatively confirms the above picture of Ru acting effectively as donors in the Ti-rich samples $Sr(Ru_{1-x}Ti_x)O_3$. Figure 9 shows for different Ti contents x the positions of the Ti K edge and the Ru K edge, respectively, as obtained from the XANES part of the x-ray absorption spectra. While the Ti K-edge position remains approximately constant, the Ru K-edge position shifts to higher energies with increasing Ti content x. This means that Ru gets more oxidized with increasing Ti content x, which is compatible with the picture of Ru acting as donor: $Ru_{Ti}^{\times} \rightleftarrows Ru_{Ti}^{\bullet} + e'$. An absolute determination of the valence state of Ru is not possible from our measurements as no standards were measured. However, for other perovskites, e.g., La_2MgRuO_6 [30] or $Pr_{0.5}Sr_{0.5}Mn_{0.9}Ru_{0.1}O_3$ [31], it was reported that the Ru K edge is shifted by ~1 eV as the Ru valence increases from 4+ to 5+. As we may assume the Ru valence to be 4+ in $SrRuO_3$ and as we observe an edge shift of ~1 eV in going from $SrRuO_3$ to $Sr(Ru_{0.1}Ti_{0.9})O_3$, we may conclude that the Ru valence has changed to 5+.

D. Power factor and solution strategy

Finally, we calculated, by using the data in Figs. 6 and 7, the power factors $\sigma\theta^2$ against oxygen activity at 973 K for different compositions and against composition x at some selective temperatures. The results are as shown in Figs. 10(a) and 10(b), respectively.

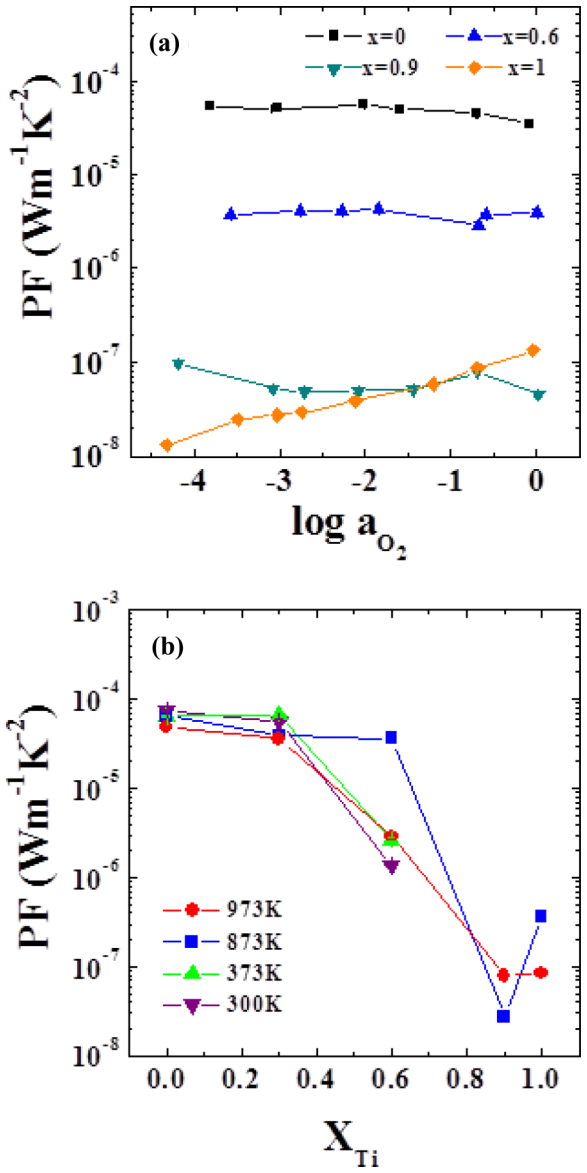

FIG. 10. (Color online) Power factor of solution $Sr(Ru_{1-x}Ti_x)O_3$ vs oxygen activity at different compositions at 973 K (a) and vs composition at selective temperatures (b). Solid lines are for visual guidance only.

It is seen that, contrary to the original expectation, the metallic end member $SrRuO_3$ exhibits the maximum power factor on the order of 10^{-4} W/mK^2 irrespective of temperature and oxygen activity as well. (The maximum value is 7.6 $\times$ 10^{-5} W/mK^2 at room temperature.) This means that the solid-solution idea for oxide thermoelectrics does not work for the present system. It is apparently because the transport properties do not vary continuously with composition of the solid solution. Instead, the solid solutions are divided into two clans, one $SrRuO_3$ like and the other $SrTiO_3$ like.

For the solid-solution idea to work or, in other words, for the power factor to be optimized between maximum conductivity and maximum thermoelectric power, both electrical properties should vary continuously across the composition. Thus, there is still a silver lining in the cloud: If the two end-member oxides having the opposite electrical properties, say, metallic versus insulating but well-coupled electronic structures, then the solid-solution idea for property hybridization will highly likely work.

IV. SUMMARY AND CONCLUSIONS

In this study, we examined the electrical conductivity and thermopower on the allegedly complete solid solution $(1\text{-}x)SrRuO_3 + xSrTiO_3$ against its composition x, temperature, and oxygen activity, in order to prove the idea of mixing a metallic conductor and an insulator for thermoelectric power-factor optimization. Contrary to the literature reports, the system does not make a complete solution leaving a miscibility gap over $0.1 < x < 0.6$. Furthermore, while the conductivity decreases monotonically with increasing x as expected, the thermopower unexpectedly varies nonmonotonically, indicating the carrier-type changes from p to n at $0.6 < x < 0.9$ and back to p at $0.9 < x < 1.0$. The solid-solution idea, thus, does not work in this system and the highest power factor is observed to be of the order of 10^{-4} W/m^{-1} K^{-2} at $x = 0$ or pure $SrRuO_3$. The carrier-type change from p to n is attributed to the gradual shift of Ru t_{2g} band to the discrete donor states of $Ru^{\bullet}_{Ti}$ with increasing x.

ACKNOWLEDGMENT

The authors thank W.-H. Lee and S.-D. Park at the Korea Electrotechnology Research Institute for their continual intellectual stimulations, D. Ahn at the Pohang Accelerator Laboratory, Korea for high-resolution XRD synchrotron measurements, and the HSAYLAB team for beam time and support.

[1] R. Venkatasubramanian, E. Siivola, T. Colpitts, and B. O'Quinn, Nature (London) **413**, 597 (2001).
[2] K. Koumoto, Y. Wang, R. Zhang, A. Kosuga, and R. Funahashi, Annu. Rev. Mater. Res. **40**, 363 (2010).
[3] L. Bocher, M. H. Aguirre, D. Logvinovich, A. Shkabko, R. Robert, M. Trottmann, and A. Weidenkaff, Inorg. Chem. **47**, 8077 (2008).
[4] T. Okuda, K. Nakanishi, S. Miyasaki, and Y. Tokura, Phys. Rev. B **63**, 113104 (2001).
[5] Y. Wang, Y. Sui, X. Wang, and W. Su, J. Phys. D: Appl. Phys. **42**, 055010 (2009).
[6] S. L. Cuffini, V. A. Macagno, R. E. Carbonio, A. Melo, E. Trollund, and J. L. Gautier, J. Solid State Chem. **105**, 161 (1993).
[7] R. F. Bianchi, J. A. G. Carrió, S. L. Cuffini, Y. P. Mascarenhas, and R. M. Faria, Phys. Rev. B **62**, 10785 (2000).
[8] K. W. Kim, J. S. Lee, T. W. Noh, S. R. Lee, and K. Char, Phys. Rev. B **71**, 125104 (2005).
[9] T. Maekawa, H. Muta, M. Uno, and S. Yamanak, J. Alloys Compd. **387**, 56 (2005).
[10] N. Keawprak, R. Tu, and T. Goto, Mater. Sci. Eng. B **161**, 71 (2009).

[11] B. H. Toby, J. Appl. Crystallogr. **34**, 210 (2001).
[12] M. Newville, J. Synchrotron Radiat. **8**, 322 (2001).
[13] D. C. Koningsberger and R. Prins, *X-Ray Absorption: Principles, Applications, Techniques of EXAFS, SEXAFS and XANES*, (Wiley, New York, 1988).
[14] H.-I. Yoo and J.-H. Hwang, J. Phys. Chem. Solids **53**, 973 (1992).
[15] M. McQuarrie, J. Am. Ceram. Soc. **38**, 444 (1955).
[16] B. J. Kennedy, B. A. Hunter, and J. R. Hester, Phys. Rev. B **65**, 224103 (2002).
[17] H. Kobayashi, M. Nagata, R. Kanno, and Y. Kawamoto, Mater. Res. Bull. **29**, 1271 (1994).
[18] H.-I. Yoo and C.-E. Lee, J. Am. Ceram. Soc. **88**, 617 (2005).
[19] S. Koerfer, R. A. de Souza, H.-I. Yoo, and M. Martin, Solid State Sci. **10**, 725 (2008).
[20] M. Shikano, T.-K. Huang, Y. Inaguma, M. Itoh, and T. Nakamura, Solid State Commun. **90**, 115 (1994).
[21] H.-I. Yoo, C.-R. Song, and D.-K. Lee, J. Electroceram. **8**, 5 (2002).
[22] F. A. Kroger and V. J. Vink, in *Solid State Physics*, edited by F. Seitz and D. Turnbull, Vol. 3 (Academic, New York, 1956), p. 307.
[23] G. H. Jonker, Philips Res. Rep. **23**, 131 (1968).
[24] P. A. Cox, R. G. Egdell, J. B. Goodenough, A. Hamnett, and C. C. Nash, J. Phys. C: Solid State Phys. **16**, 6221 (1983).
[25] E. Heifets, R. I. Eglitis, E. A. Kotomin, J. Maier, and G. Borstel, Surf. Sci. **513**, 211 (2002).
[26] H.-C. Chen, C.-W. Huang, J. C. S. Wu, and S.-T. Lin, J. Phys. Chem. C **116**, 7897 (2012).
[27] H. Matsumoto, D. Murakami, T. Shimura, S.-I. Hashimoto, and H. Iwahara, J. Electroceram. **7**, 107 (2001).
[28] C. Wagner, Prog. Solid State Chem. **7**, 1 (1972).
[29] A. Rothschild, S. J. Litzelman, H. L. Tuller, W. Menesklou, T. Schneider, and E. Ivers-Tiffée, Sens. Actuators B **108**, 223 (2005).
[30] J.-H. Choy, J.-Y. Kim, S.-H. Hwang, S.-J. Kim, and D. Grared, Inter. J. Inorg. Mater. **2**, 61 (2000).
[31] J. S. Kim, B. H. Kim, D. C. Kim, M. G. Kim, A. Maignan, B. Raveau, and Y. W. Park, Phys. Scr., T **115**, 498 (2005).